THE JOURNAL OF PHYSICAL CHEMISTRY Letters

Letter

pubs.acs.org/JPCL

Translation Symmetry Breakdown in Low-Dimensional Lattices of Pentagonal Rings

Paul Avramov,*[,†] Victor Demin,[‡] Ming Luo,[§] Cheol Ho Choi,[†] Pavel B. Sorokin,[∥] Boris Yakobson,[§] and Leonid Chernozatonskii[‡]

[†]Department of Chemistry and Green-Nano Materials Research Center, College of Natural Sciences, Kyungpook National University, 1370 Sankyuk-dong, Buk-gu, Daegu 702-701, Republic of Korea

[‡]N.M.Emanuel Institute of Biochemical Physics, Russian Academy of Sciences, Kosugin 4, 119334 Moscow, Russia

[§]Department of Materials Science and NanoEnigeering, Rice University, Houston, Texas 77005, United States

[∥]National University of Science and Technology MISiS, Moscow 119049, Russian Federation

Supporting Information

ABSTRACT: The mechanism of translation symmetry breakdown in newly proposed low-dimensional carbon pentagon-constituted nanostructures (e.g., pentagraphene) with multiple sp^2/sp^3 sublattices was studied by GGA DFT, DFTB, and model potential approaches. It was found that finite nanoclusters suffer strong uniform unit cell bending followed by breaking of crystalline lattice linear translation invariance caused by structural mechanical stress. It was shown that 2D sp^2/sp^3 nanostructures are correlated transition states between two symmetrically equivalent bent structures. At DFT level of theory the distortion energy of the flakes (7.5×10^{-2} eV/atom) is much higher the energy of dynamical stabilization of graphene. Strong mechanical stress prevents stabilization of the nanoclusters on any type of supports by either van der Waals or covalent bonding and should lead to formation of pentatubes, nanorings, or nanofoams rather than infinite nanoribbons or nanosheets. Formation of two-layered pentagraphene structures leads to compensation of the stress and stabilization of flat finite pentaflakes.

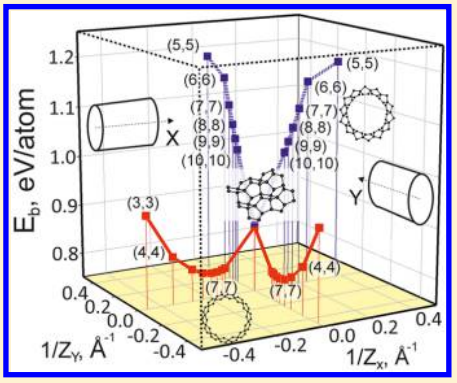

Recently, a number of pentagon-constituted perfect 2D nanostructures of mixed sp^2-sp^3 hybridization of constituted atoms (see for example, pentagraphene,[1] pentagonal silicon dicarbide $pSiC_2$,[2] pentagonal p-B_2N_4, p-B_4N_2, and p-AgN_3[3]) with multiple sublattices were theoretically introduced using periodic boundary conditions (PBC) GGA DFT electronic structure calculations. 2D pentagraphene, $pSiC_2$, and p-B_2N_4 have three-layer-thick structure and resemble Cairo pentagonal tilling with central sp^3 carbon,[1] silicon,[2] or boron[3] sublattice and two perpendicular symmetrically nonequivalent sp^2 carbon,[1,2] nitrogen[3] dimers (trimers in the case of p-AgN_3) sublattices located in top and bottom layers.

In particular, the atomic and electronic structure and stability of pentagraphene[1] (Figure 1a,b) were studied by electronic structure calculations and ab initio molecular dynamics simulations using PBC PW GGA DFT approach. Pentagraphene can be designed by exfoliation of one unit cell-thick film from T12-carbon.[4] Pentagon-based carbon nanotubes, formed by rolling of pentagraphene and multilayered T12-carbon films composed by two and four unit cells in (001) direction proved to be structurally stable as well. In contrast with graphene,[5] pentagraphene (Figure 1), $pSiC_2$, p-B_2N_4, and p-B_4N_2 have nonzero thickness (1.2 Å for pentagraphene[1] and 1.3 Å for $pSiC_2$[2]) and consist of three sublattices, with two top and bottom ones composed by mutually perpendicular dimers. The third sublattice is formed by one central sp^3 carbon,[1] silicon,[2] boron, or nitrogen[3] atoms, which merge the entire structures. The carbon/nitrogen/boron dimer sublattices are mutually perpendicular to each other and may create uncompensated structural stresses caused by the symmetry of the unit cells.

In contrast with isotropic hexagonal graphene and *h*-BN, for symmetry anisotropic low-dimensional MgB_x fullerenes and nanotubes,[6,7] zigzag *h*-BN, SiC and single-side fluorinated graphene nanoribbons[8] and CF_2 nanoshells,[9] the bending effects of the structural units by uncompensated mechanical stress have been already observed. For example, unilateral fluorination of the carbon lattice causes structural asymmetry and significant energy first derivative in the vicinity of zero curvature of C_2F layer.[9] Uncompensated structural stress of flat C_2F layer creates finite internal bending torque and large final curvature of the sheet making formation of C_xF polygonal nanotubes energetically favorable.

The effect of lowering symmetry is very common in chemistry and material science (see, for example ref 10) and can be caused by different reasons. In general, to reveal true symmetry of a molecule or solid one should drop symmetry

Received: September 4, 2015
Accepted: October 23, 2015

DOI: 10.1021/acs.jpclett.5b02309
J. Phys. Chem. Lett. 2015, 6, 4525−4531

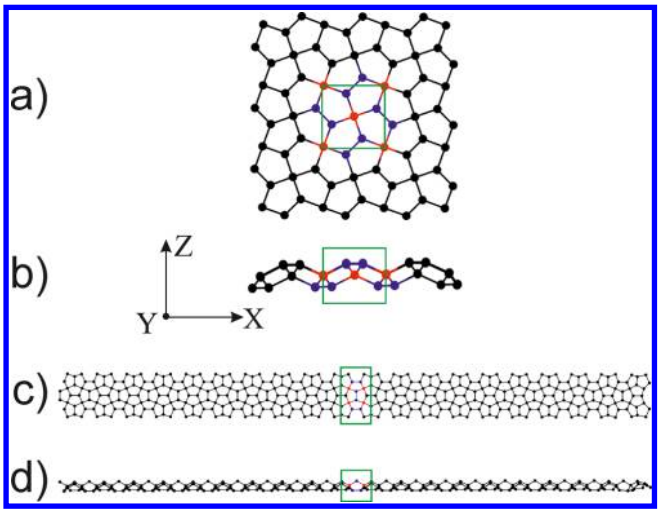

Figure 1. Top (a) and side (b) projections of 2D pentagraphene and 1D pentaribbon (c, d) calculated using PBC approach. Carbon atoms of sp^3 sublattice are depicted in red, the sp^2 carbon dimers of the top and bottom subblattices are depicted in blue, the unit cells of pentagraphene and pentaribbon are marked by green rectangles.

restrictions to avoid artificial symmetry constraints (in particular this technique is realized for Hessian evaluation). The periodic boundary approach, which is an implementation of translation symmetry for solid state physics,[11] linearly multiplies images of the unit cells along specific crystallographic directions. Previously, it was shown that linear translation symmetry is not suitable to reproduce curved low-dimensional nanoclusters, which suffer the lack of translation symmetry.[8] Because the phonons are collective excitations in a linear periodic elastic arrangement of atoms or molecules, for curved nanostructures the calculations of phonon frequencies cannot prove whether or not an extreme point on potential energy surface is a local or global minimum, but not a transition state, conical intersection, or higher order saddle point. The only way to reveal true symmetry for potentially curved nanostructures is to drop translation symmetry and calculate finite clusters of arbitrary dimensions.[8]

To study the atomic and electronic structure of pentagraphene and $pSiC_2$ nanoclusters (flakes, nanorings, nanotubes, and two-layered flakes, Figures 2, 3, and 4), ab initio GGA DFT PBE[12] calculations of finite clusters with standard norm-conserving pseudopotentials, flexible numerical LCAO multiple zeta + polarization orbital basis sets were used. The real-space mesh cutoff was set to 175 Ry. For the sake of comparison a set of pristine 2D pentagraphene, two-layered 2D pentagraphene and 14 perfect 1D pentatubes (direct (3,3) and (4,4) pentatubes, and both direct and inverted (5,5), (6,6), (7,7)

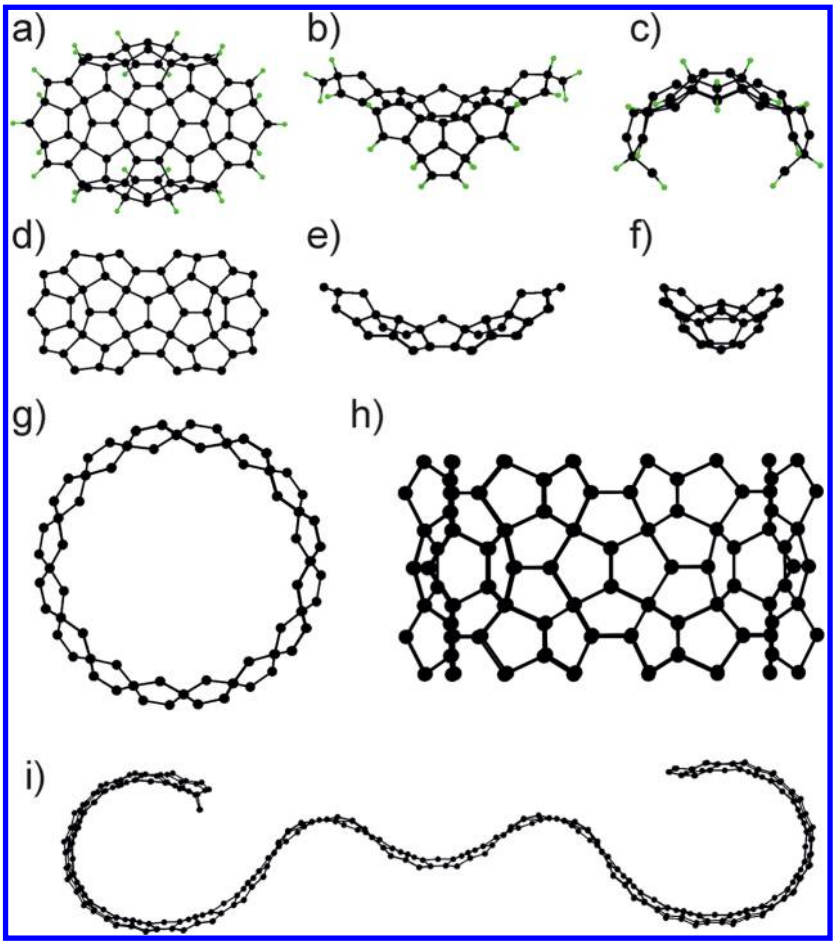

Figure 2. (a), (b), and (c) Top and two side views of pentagraphene $C_{72}H_{28}$ flake. (d), (e), and (f): Top and two side views of pentagraphene C_{52} flake, the main building block of pentarings and pentatubes. (g) and (h) (8,8) pentaring in two projections. The cutaway (h) is presented for clarification of the structure (i): MM+ optimized structure of finite pentagraphene nanoribbon C_{400} of 20 unit cell length and 7.3 Å width. Carbon atoms are depicted in black; hydrogen atoms are depicted in green.

DOI: 10.1021/acs.jpclett.5b02309
J. Phys. Chem. Lett. 2015, 6, 4525−4531

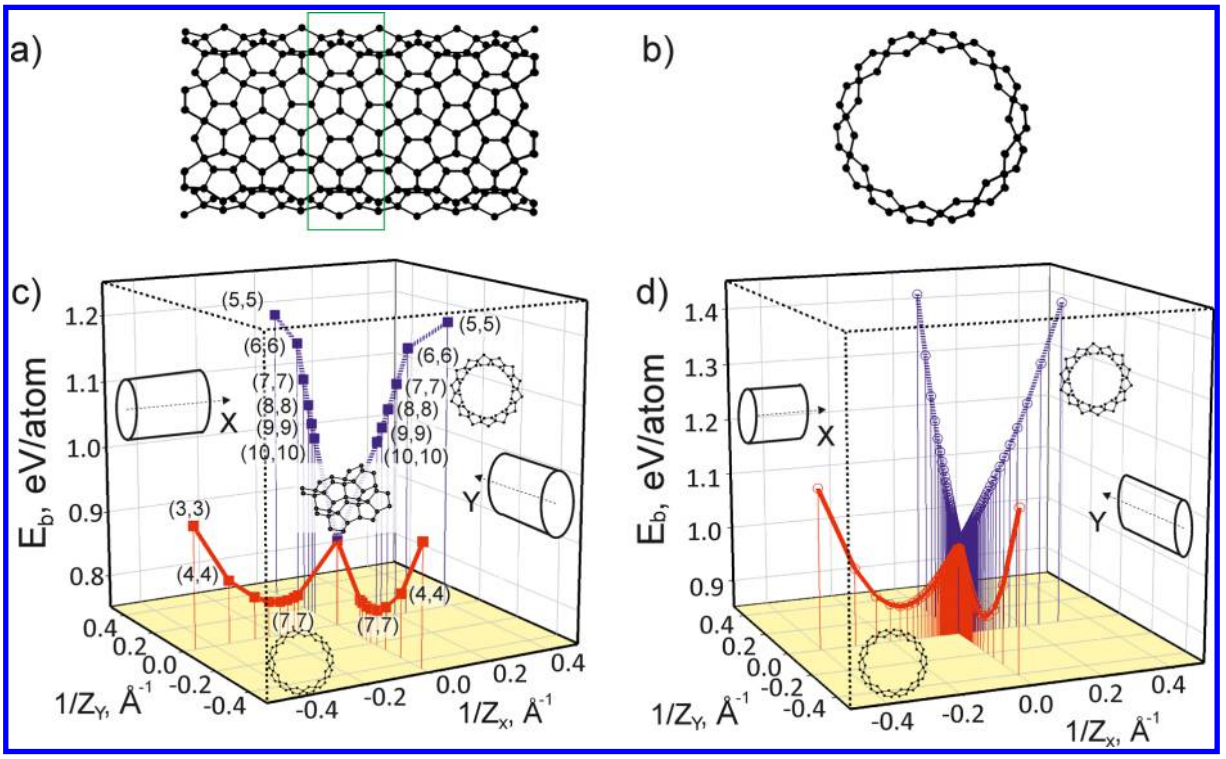

Figure 3. (a), (b) Side and top views of the most stable direct pentatube (7,7) with inner dimers parallel to the tube axis. A cross section (a) of the nanotube is presented for simplicity. The main building block of the nanotube consisting of seven pentagraphene unit cells is marked by green rectangular. (c) Relative DFT binding energies per atom (E_b) of direct (3,3)−(10,10) (red parts of the curves) and inverted (5,5)−(10,10) (blue parts) pentatubes rolled along *X* (top carbon dimers) and *Y* (bottom carbon dimmers) directions. (d) Relative DFTB binding energies per atom (E_b) of direct (3,3)−(360,360) (in red) and inverted (in blue) (4,4)−(360,360) pentatubes rolled along *X* (top carbon dimers) and *Y* (bottom carbon dimmers) directions. Crossings of red and blue parts of *X* and *Y* wings of potential energy surfaces correspond to pentagraphene with zero curvature (panel c). The *X* and *Y* orientations of the pentatube rolling are presented for clarity. *X* and *Y* directions and perpendicular cross sections of both direct and inverted pentatubes are presented at left and right of panels c and d. The binding energy of graphene at GGA DFT PBC and DFTB levels of theory are taken as references (E_b = 0 eV). E_b of pentagraphene is equal to 0.86 and 1.01 eV/atom for DFT and DFTB levels of theory, respectively.

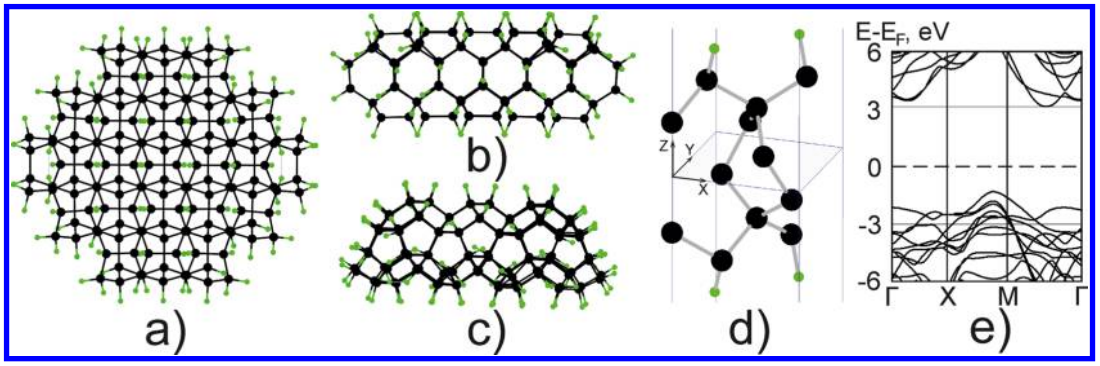

Figure 4. (a), (b), (c) Bilayered AB pentagraphene flake $C_{158}H_{108}$, top and two side views, respectively. (d), (e): Unit cell and band structure of bilayered AB pentagraphene. Carbon atoms are depicted in black; hydrogen atoms are depicted in green.

(8,8), (9,9), and (10,10) pentatubes, the details of the atomic structure are described below) were calculated using PBC GGA DFT approach. 0D, 1D, and 2D system was separated from its periodic images by a vacuum distance of 10 Å. To calculate the equilibrium atomic structures, the Brillouin zone was sampled according to the Monkhorst−Pack scheme[13] with a *k*-points density of 0.06 Å^{-1}. In the course of the atomic structure minimization, structural relaxation was carried out until the change in total energy was less than 10^{-4} eV, or forces acting on each atom were less than 10^{-3} eV Å^{-1}. The atomic and electronic structure calculations were carried out by SIESTA code.[14] In addition, an extended pentagraphene nanoribbon C_{400} of 20 unit cell length and 7.3 Å width (Figure 1c,d) was optimized using classical MM+ potential (Figure 2i).

In order to obtain a broader picture of the potential energy landscape, especially in the vicinity of the hypothetical planar pentagraphene, one needs to explore it at very small curvatures. This is unaffordable for DFT, due to exceedingly large number of atoms in the unit cell. To address this, we additionally performed the energy computations within density functional tight binding (DFTB) approximation,[15] augmented by a symmetry-adapted scheme for the electronic systems,[16] as

DOI: 10.1021/acs.jpclett.5b02309
J. Phys. Chem. Lett. 2015, 6, 4525−4531

pioneered in ref 17. The planar pentagraphene and two sets of pentatubes (one can find the structural details below) with indexes from (3,3) to (360,360) were calculated using DFTB code, described in refs 15 and 18. The lattice constant for PBC DFTB calculations was equal to 5.148 Å. For all calculations, the same C_{12} unit cell was used. To design all pentatubes, the rotary symmetry was applied for circumference multiplication of the unit cells with bending angles equal to $(360°/n)$, where n is a nanotube index. For example, for energy preferable (7,7) pentatube the bending angle was equal to $(360°/7) = 51.43°$. All structures were relaxed until energy change less than 10^{-6} au.

It was found that finite pentagraphene and $pSiC_2$ flakes suffer strong distortion of crystalline lattice due to uncompensated mechanical stress caused by orthogonal sp^2 lattices. The stress leads to complete breakdown of linear translation symmetry with formation of irregular curved structures, nanorings, or pentatubes, which prevents the formation of infinite 2D pristine pentagraphene or 1D pentagraphene ribbons. In contrast, formation of two-layered T12 films of finite thickness leads to compensation of bending stress by opposing stretching deformation caused by significant thickness of two-layered film. As a result, it leads to stabilization of two-layered flakes (Figure 4). It was found that (7,7) pentatube is the most energetically stable due to the matching of pentagraphene and pentatube (7,7) curvatures (Figure 3c,d). In one-electron approximation, the plot (Figure 3c,d) of binding energy per carbon atom against curvatures of perfect 1D pentatubes and 2D pentagraphene (for pentagraphene the curvature is equal to 0 by definition) demonstrates that pentagraphene can be a transition state between two equivalent curved structures, or it may represent more complex cases of a conical intersection or higher order saddle point between two curved structures. Many-electron consideration of DFTB potential energy curves of low curvature clusters unambiguously proves that pentagraphene is the only one transition state on potential energy surface of mechanical bending of pentagraphene. Optimized structures of the key nanoclusters can be found in Supporting Information.

The pentagraphene flake $C_{72}H_{28}$ (Figure 2a,b,c) displays distinctive saddle structure of 0.226 $Å^{-1}$ and 0.053 $Å^{-1}$ curvatures in perpendicular directions. The anisotropy is caused by the different number of sp^2 carbon dimers located in the top (three) and bottom (two) pentagraphene sublattices. At GGA DFT level of theory the HOMO−LUMO gap of $C_{72}H_{28}$ flake is equal to 3.01 eV. For the sake of comparison, the PBC GGA DFT calculation of infinite flat pentagraphene (Figure 1a,b) reveals 0 $Å^{-1}$ curvature (perfect 2D plane) and 2.10 eV band gap.

The classical MM+ potential optimization of free-standing pentagraphene nanoribbon C_{400} of 20 unit cell length (10 nm) and 7.3 Å width (Figure 2i) clearly demonstrates induced complex curvature of finite extended nanocluster. Both sides of the nanoribbon suffer distinctive curvatures, which roll the nanoribbon. The complex curvature of the nanoribbon is caused by structural irregularities of initial cluster before atomic structure optimization.

The $pSiC_2$ $Si_{24}C_{48}H_{28}$ flake was designed by substituting of all sp^3 carbon atoms of $C_{72}H_{28}$ (Figure 2) by silicon. As in the case of pentagraphene flake $C_{72}H_{28}$, the $pSiC_2$ $Si_{24}C_{48}H_{28}$ nanocluster demonstrates distinctive 0.170 and 0.024 $Å^{-1}$ curvatures. The optimized $Si_{24}C_{48}H_{28}$ flake structure can be found in Supporting Information.

The (n,n) pentatubes[1] (Figure 3a,b) can be designed by rolling up the pentagraphene plane along chiral vectors $n = m$ in X and Y in-plane directions (coordinate system is represented in Figure 1, each direction is parallel to one set of the dimers). Also, the direction of rolling along Z orientation can be positive or negative. Both top and bottom sides of pentagraphene are structurally equivalent and each way of rolling can produce two types of pentatubes with inner dimers parallel (direct pentatube, Figure 3b,c,d) or perpendicular (inverted type, Figure 3c,d) to the main axis of the pentatube. So, pentagraphene can be rolled into two (direct and inverted) types of pentatubes oriented along two perpendicular X and Y directions above or below the $X-Y$ plane, respectively.

The unit cell of the most stable direct (7,7) pentatube consists of C_{84} ring. In order to estimate the energetic stability of pentagraphene structures, the corresponding formation energies per carbon atom were calculated in accordance with the formula

$$E_b = \frac{E_{tot} - N_C E_C}{N_C}$$

where E_{tot} is total energy of system, N_c and E_c are number of carbon atoms in unit cell and energy of isolated carbon atom, respectively.

The direct (n,n) pentatubes are energetically preferable in comparison with inverted ones (Figure 3c,d). Rolling parallel to the top dimers (X orientation) produces direct pentatubes with positive Z coordinate values (above the pentagraphene plane), which are formally coincide with the radii R of the tubes. For direct X oriented top pentatubes, we can determine the curvature as $D^d_{top} = (1/R^d_x) = (1/Z_x)$. The inverted X oriented top tubes rolled along top dimers have negative Z values (in that case $R^i_x = -Z_x$) and respective curvatures $D^i_{top} = (1/R^i_x) = (1/-Z_x)$. The direct and inverted bottom pentatubes (Y orientation of rolling) can be determined in the same way with $R^d_y = -Z_y$ and $R^i_y = Z_y$, respectively. The dependencies of the pentatube energies of both direct and inverted types rolled along X and Y directions, respectively, are presented in Figure 3c (DFT calculations of (3,3)−(10,10) direct and (5,5)−(10,10) inverted tubes) and Figure 3d (DFTB calculations of (3,3)−(360,360) direct and inverted (4,4)−(360,360) tubes).

DFT calculations of pentatube main building block C_{52} flake (Figure 2d,e,f) and pentagraphene (8,8) ring (Figures 2g,h) reveal the same saddle structural feature. Mechanical stress caused by the carbon dimers leads to nanocluster bending with 0.131 $Å^{-1}$ curvature. The distinctive curvature of the finite pentagraphene flake may cause closure of the opposite edges with formation of finite-length nanoring.

The pentatube fragments and binding energies against curvature of the pentatubes and pentagraphene (the curvature of pentagraphene is equal to 0 by definition) are presented in Figure 3a,b and Figure 3c,d, respectively. Red and blue parts of both X- and Y-oriented wings in Figure 3c (DFT, (3,3)−(10,10) pentatubes) and 3d (DFTB, (3,3)−(360,360) tubes) correspond to direct and inverted pentatubes, respectively. Perfectly flat pentagraphene has zero curvature (infinite Z value) and corresponds to the crossing of one-electron (DFT and DFTB) potential energy curves (PEC, Figures 3c, 3d). It is necessary to note that at one-electron level of theory (both DFT and DFTB) perfectly flat pentagraphene is just a regular point on a potential energy surface with non-zero derivative,

DOI: 10.1021/acs.jpclett.5b02309
J. Phys. Chem. Lett. 2015, 6, 4525−4531

rather than an extreme point (global or local minimum or transition state).

The classical von Neumann−Wigner theorem[19] implies avoiding crossing rule for symmetric eigenvalues[20] of one-parameter Hermitian matrix representing physical observable. In particular, for one-parameter potential energy curves of diatomics, it means the eigenvalues of different configurations do not cross and form two hyperbola-like noncrossing potential energy curves representing a lower-energy transition state (local maximum) and local minimum of the excited state.

For typical one-parameter case of bending of perfect 2D pentagraphene in two symmetrically equivalent perpendicular X and Y directions, two equivalent one-electron potential energy curves cross each other in the vicinity of perfectly flat 2D pentagraphene. The electronic correlations[20] transform two crossing terms into ground state PEC (red curves, Figure 3c,d) with two equivalent global minima corresponding to perpendicularly oriented direct (7,7) pentatubes and one correlated transition state of perfectly flat 2D pentagraphene. At multielectron level of theory,[20] the second PEC (blue curves, Figure 3c,d) corresponds to the first excited state with perfectly flat 2D pentagraphene as a local minimum just above PEC maximum of the ground state.

The GGA DFT PBC electronic structure calculations of direct (3,3), (4,4), (5,5), (6,6), (7,7), (8,8), (9,9), and (10,10) and inverted (5,5), (6,6), (7,7), (8,8), (9,9), and (10,10) pentatubes reveal distinctive minimum of E_b binding energy per atom for direct (7,7) pentatube (Figure 3c), which is caused by the best matching of the (7,7) pentatube curvature (0.191 $Å^{-1}$) with the curvature of the C_{52} flake (0.131 $Å^{-1}$). The uncompensated mechanical stress of finite pentaflakes leads to breakdown of linear translation symmetry by creating equivalent curved structural units, which can form perfect nanorings or pentatubes. The width of semiconducting band gap of direct (7,7) pentatube is equal to 2.46 eV.

DFTB calculations of large diameter direct and inverted pentatubes (up to (360,360) tube indexes) of very low curvatures (Figure 3d) reveal very smooth behavior of potential energy curves in the vicinity of pentagraphene. Increasing of the pentatube diameter leads to smooth approaching of the pentatube binding energies to the binding energy of pentagraphene for both direct and inverted types. The DFTB calculations perfectly fill the gap in DFT potential energy curves (Figure 3c) for large-diameter pentatubes.

Large diameter pentatubes with arbitrary chiral angle α (small bending along arbitrary direction $\vec{K} = \vec{i}\cos\alpha + \vec{j}\sin\alpha$, where $\vec{i}$ and $\vec{j}$ are coordinate basis vectors) can be considered as a superposition of two deformations along X and Y orientations. Let us consider for simplicity an orthonormal $\{\Psi^k_G(n,n)\}$ set. Pentagraphene has two perpendicular carbon dimers on the top and bottom of the unit cell, so a state function of pentagraphene of small bending along $\vec{K}$ direction corresponds to a superposition of the state functions of one direct (n,n) and one inverted (n,n) pentatubes $\Phi(\alpha) = \cos\alpha \times \Psi^d_G(n,n) + \sin\alpha \times \Psi^i_H(n,n)$, where G can be either X or Y and H can be Y or X, respectively. So, in general, rotating the pentatube chiral angle α one can perform the following transformations:

$$\Psi^d_X(n,n) \rightarrow \Psi^i_Y(n,n);$$
$$\Psi^i_X(n,n) \rightarrow \Psi^d_Y(n,n);$$
$$\Psi^i_Y(n,n) \rightarrow \Psi^d_X(n,n);$$
$$\Psi^d_Y(n,n) \rightarrow \Psi^i_X(n,n)$$

Once again, let us consider two symmetrically equivalent potential energy surfaces with the state functions of $\Phi_X(\alpha_X) = \cos\alpha_X \times \Psi^d_X(n,n) + \sin\alpha_X \times \Psi^i_Y(n,n)$ and $\Phi_Y(\alpha_Y) = \cos\alpha_Y \times \Psi^d_Y(n,n) + \sin\alpha_Y \times \Psi^i_X(n,n)$. For $\alpha_X = \alpha_Y = l \times (\pi/4)$ (l = 1, 3, 5, 7) chiral angles, the state functions are equal to each other because of symmetrical reasons

$$\Phi_X(\alpha_X) = \Phi_Y(\alpha_Y) = \frac{1}{\sqrt{2}}(\Psi^d_X(n,n) + \Psi^i_Y(n,n)) = \frac{1}{\sqrt{2}}(\Psi^d_Y(n,n) + \Psi^i_X(n,n))$$

It means that the potential energy surfaces cross each other in four symmetrically equivalent linear seams with chiral angles $(\pi/4)$, $(3/4)\pi$, $(5/4)\pi$, $(7/4)\pi$. Let's consider for simplicity a case of $\alpha = (\pi/4)$.

Because of structural features of pentagraphene, the energies of inverted pentatubes are always higher than the energies of direct ones, so $E^i_G(n,n) > E^d_H(n,n)$ for all pentatube indexes (Figure 3d). The difference $E^i_Y(n,n) - E^d_X(n,n)$ is always positive and monotonically decreases with increasing of the n index. Using the orthonormal properties of $\{\Psi^k_G(n,n)\}$ set, the energy of a pentatube with chiral angle $\alpha = (\pi/4)$ can be expressed as $E(\alpha) = (1/2)\,(E^d_X(n,n) + E^i_Y(n,n))$. For large diameter pentatubes (Figure 3d), we can always write

$$E^d_X(n,n) = E^d_Y(n,n) < E_{PG}$$
$$E^i_X(n,n) = E^i_Y(n,n) > E_{PG}$$

where E_{PG} is pentagraphene energy. These equations mean that for large diameter pentatubes with chiral angles of $(\pi/4)$, $(3/4)\pi$, $(5/4)\pi$, $(7/4)\pi$ (which belong to seam regions) the pentatube energies and energies of seams as well are always higher than the energy of flat 2D pentagraphene.

For one-parameter $\Psi^d_X(n,n) \rightarrow \Psi^d_Y(n,n)$ transformation (see above) avoiding crossing rule[19] leads to repulsion of both ground and first excited states with formation of transition state of finit energy splitting. For small curvatures and chiral angles the energy of electronic correlations is just a small correction to one-electron total energy and the potential energy curve of $\Psi^d_X(n,n) \rightarrow \Psi^d_Y(n,n)$ transformation is just a part of total potential energy surface of $\Phi_X(\alpha_X) \rightarrow \Phi_Y(\alpha_Y)$ transformation. As it was shown, the energy of one-electron seam regions (chiral angles $(\pi/4)$, $(3/4)\pi$, $(5/4)\pi$, $(7/4)\pi$) are always higher than the energy of pentagraphene. It means that complete potential energy surface of the correlated ground state of pentagraphene has the only one transition state which corresponds to perfectly flat 2D pentagraphene (Figures 3c, 3d). For the low curvature region, pentagraphene is a correlated system for which electronic correlations determine the main features of the electronic structure. In contrast, the first excited state has minimum in the vicinity of perfectly flat 2D pentagraphene.

At GGA DFT PBC level of theory the binding energy of plane pentagraphene is 7.5×10^{-2} eV/atom higher the E_b of (7,7) pentatube due to uncompensated structural stress. All

DOI: 10.1021/acs.jpclett.5b02309
J. Phys. Chem. Lett. 2015, 6, 4525−4531

inverted pentatubes and narrowest (3,3) direct pentatube have binding energies higher the binding energy of pentagraphene (8.76×10^{-1} eV/atom in respect to pristine graphene, Figure 3c). Perfect 2D pentagraphene is well-defined correlated transition state between two symmetrically equivalent perpendicularly oriented global minima of curved structures with curvatures equal to 0.191 $Å^{-1}$.

The energy gain caused by structural relaxation of a flat finite pentagraphene fragment can be determined as a number of carbon atoms multiplied by the relative energy of pentagraphene in respect with the energy of (7,7) pentatube (7.5×10^{-2} eV/atom, see above). For example, for $C_{72}H_{28}$ pentagraphene cluster the energy gain or energy of corrugation is equal to 1.2519×10^{2} kcal/mol (7.5×10^{-2} eV/atom × 72 atoms ×23.0604), which is 10^{2}−10^{3} times stronger the energy of van der Waals (vdW) interactions ($9.6 \times 10^{-1} - 9.6 \times 10^{-2}$ kcal/mol[21]) and 1.5 higher the average energy of single carbon−carbon covalent bond (8.3×10^{1} kcal/mol[22]).

The high corrugation energy makes a substrate-derived formation of extended flat 1D or 2D fragments of pentagraphene practically impossible. The structural stress is so high, that it would be impossible to fix noncorrugated cluster on any surface using either vdW or covalent bonding. The structure should be immediately distorted, all bonds of any type with the substrate should be destroyed and a small piece of carbon nanofoam[23] should be created.

For perfect low dimensional (1D and 2D) crystalline lattices, thermal fluctuations should destroy long-range order, resulting in melting of the crystalline lattice.[24] Stabilization of 1D and 2D nanoclusters occurs due to several reasons: First, most nanoclusters are deposited on different types of supports or they form quasi-3D structures like nanotube bundles. The second type of stabilization is caused by breakdown of the periodicity by creating lattice defects. And the third type of stabilization is realized for free-standing perfect 2D graphene due to formation of corrugated structure with very long wavelengths (100 Å $\leq L \leq$ 250 Å) and height of 10 Å.[25] According to simple evaluations, based on de Broglie wavelength, the energy of graphene stabilization (see Supporting Information) is very low and equal to $2.445 \times 10^{-14} - 6.027 \times 10^{-16}$ eV/atom. The energy of structural distortion (7.5×10^{-2} eV/atom, see above) is is $3.271 \times 10^{12} - 1.244 \times 10^{14}$ times greater the energy of stabilization of 2D pristine graphene.

Finally, the bilayered $C_{158}H_{108}$ flake in AB configuration (Figure 4a−c) as well as infinite 2D bilayered AB T12 film (square $C_{12}H_4$ unit cell, translation vector a = 3.47 Å, Figure 4d)[1] were calculated using GGA DFT approach. According to ref 1, the AB configuration of T12 carbon film is formed by two pentagraphenes, one of which is rotated by 180° along in respect to another. In AB configuration, both layers form a united superstructure of 4.66 Å thickness with two perpendicular sets of the sp^2 carbon dimers, with two sp^2 sublattices in each set. Resulting bending force caused by perpendicular sp^2 dimers creates strong opposing stretching response due to significant finite thickness of bilayered pentagraphene. As a result, both bending and stretching forces compensate each other and the nanocluster keeps it perfect 2D planar structure. The HOMO−LUMO energy difference of $C_{158}H_{108}$ nanocluster is equal to 5.41 eV. For the infinite bilayered AB T12 film, an indirect 4.40 eV band gap was detected (Figure 4e).

Using model potential, DFTB and GGA DFT electronic structure calculations it was found that pentagraphene and $pSiC_2$ suffer translation symmetry break caused by uncompensated mechanical stress created by two mutually orthogonal sp^2 sublattices of carbon dimers on the opposite sides of the nanoclusters. Instead of linear translated invariant unit cells, the stress leads to formation of uniformly curved repetitive structural units that can be combined in irregular nanoclusters of saddle shape, pentarings, or pentatubes. It was found that perfect 2D pentagraphene is a correlated transition state between two symmetrically equivalent perpendicularly oriented bent structures of 0.191 $Å^{-1}$ curvature. The energy of structural stress (7.5×10^{-2} eV/atom) is much higher than the energies of dynamical stabilization of perfect graphene, vdW forces or sp^3 C−C covalent bond, which makes substrate-derived formation of extended 1D and 2D pentagraphene structures practically impossible. The curved structure of pentagraphene should result in formation of pentagraphene nanofoam, pentananorings, and pentatubes. Among many possible structures, pentatube (7,7) is energetically favorable due to coincidence of the finite flake and pentatube curvatures. It was confirmed that bilayered AB pentagraphenes are structurally stable due to compensation of the stress by two perpendicular sets of mutually parallel sp^2 carbon sublattices.

■ ASSOCIATED CONTENT

Supporting Information

The Supporting Information is available free of charge on the ACS Publications website at DOI: 10.1021/acs.jpclett.5b02309.

Estimation of corrugation energy of graphene.[25] (PDF)

GGA DFT optimized coordinates of the pentagon-constituted carbon nanostructures. (PDF)

■ AUTHOR INFORMATION

Corresponding Author

*E-mail: paul@iph.krasn.ru.

Notes

The authors declare no competing financial interest.

■ ACKNOWLEDGMENTS

P.A. acknowledges KNU Research Fund, 2014. V.D., P.B.S., and L.C. acknowledge the support of Program F7, project 318617-FAEMCAR. P.B.S. acknowledges the financial support of the Ministry of Education and Science of the Russian Federation in the framework of Increase Competitiveness Program of NUST "MISiS" (No K2-2015-033). Work at Rice University (M.L.) was supported by the AFOSR MURI grant FA9550-12-1-0035. All calculations were performed using the resources of the Interdepartmental Supercomputer Center (ISC) and the Lomonosov Supercomputer Complex, Moscow State University.[26]

■ REFERENCES

(1) Zhang, S.; Zhou, J.; Wang, Q.; Chen, X.; Kawazoe, Y.; Jena, P. Penta-graphene: A New Carbon Allotrope. *Proc. Natl. Acad. Sci. U. S. A.* **2015**, *112*, 2372−2377.

(2) Lopez-Bezanilla, A.; Littlewood, P. B. σ-π-Band Inversion in a Novel Two-Dimensional Material. *J. Phys. Chem. C* **2015**, *119*, 19469−19474.

(3) Yagmurcukardes, M.; Sahin, H.; Kang, J.; Torun, E.; Peeters, F. M.; Senger, R. T. Pentagonal Monolayer Crystals of Carbon, Boron Nitride, and Silver Azide. *J. Appl. Phys.* **2015**, *118*, 104303.

DOI: 10.1021/acs.jpclett.5b02309
J. Phys. Chem. Lett. 2015, 6, 4525−4531

(4) Zhao, Z.; Tian, F.; Dong, X.; Li, Q.; Wang, Q.; Wang, H.; Zhong, X.; Xu, B.; Yu, D.; He, J.; Wang, H.-T.; Ma, Y.; Tian, Y. Tetragonal Allotrope of Group 14 Elements. *J. Am. Chem. Soc.* **2012**, *134*, 12362−12365.
(5) Novoselov, K. S.; Geim, A. K.; Morozov, S. V.; Jiang, D.; Zhang, Y.; Dubonos, S. V.; Grigorieva, I. V.; Firsov, A. A. Electric Field Effect in Atomically Thin Carbon Films. *Science* **2004**, *306*, 666−669.
(6) Sorokin, P. B.; Chernozatonskii, L. A.; Avramov, P. V.; Yakobson, B. I. Magnesium Boride Nanotubes: Relative Stability and Atomic and Electronic Structure. *J. Phys. Chem. C* **2010**, *114*, 4852−4856.
(7) Chernozatonskii, L. A. Diboride Bifullerenes and Binanotubes. *JETP Lett.* **2001**, *74*, 335−339.
(8) Avramov, P. V.; Fedorov, D. G.; Sorokin, P. B.; Sakai, S.; Entani, S.; Ohtomo, M.; Matsumoto, Y.; Naramoto, H. Intrinsic Edge Asymmetry in Narrow Zigzag Hexagonal Heteroatomic Nanoribbons Causes their Subtle Uniform Curvature. *J. Phys. Chem. Lett.* **2012**, *3*, 2003−2008.
(9) Kudin, K. N.; Scuseria, G. E.; Yakobson, B. I. C_2F, BN, and C Nanoshell Elasticity from ab initio Computations. *Phys. Rev. B: Condens. Matter Mater. Phys.* **2001**, *64*, 235406.
(10) Shriver, D. F.; Atkins, P. W. *Inorganic Chemistry*, 3rd ed.; Oxford University Press: Oxford, U.K., 1999.
(11) Kittel, C. *Introduction to Solid State Physics*, 8th ed.; John Wiley & Sons, Inc.: Hoboken, NJ, 2004, ISBN: 047141526X.
(12) Perdew, J. P.; Burke, K.; Ernzerhof, M. Generalized Gradient Approximation Made Simple. *Phys. Rev. Lett.* **1996**, *77*, 3865−3868.
(13) Monkhorst, H. J.; Pack, J. D. Special Points for Brillouin-zone Integrations. *Phys. Rev. B* **1976**, *13*, 5188−5192.
(14) Soler, J. M.; Artacho, E.; Gale, J. D.; Garcia, A.; Junquera, J.; Ordejon, P.; Sanchez-Portal, D. The Siesta Method for ab initio Order-N Materials Simulation. *J. Phys.: Condens. Matter* **2002**, *14*, 2745−2779.
(15) Rurali, R.; Hernandez, E. Trocadero: A Multiple-algorithm Multiple-model Atomistic Simulation Program. *Comput. Mater. Sci.* **2003**, *28*, 85−106.
(16) Zhang, D.-B.; Seifert, G.; Chang, K. Strain-Induced Pseudomagnetic Fields in Twisted Graphene Nanoribbons. *Phys. Rev. Lett.* **2014**, *112*, 096805.
(17) White, C. T.; Robertson, D. H.; Mintmire, J. W. Helical and Rotational Symmetries of Nanoscale Graphitic Tubules. *Phys. Rev. B: Condens. Matter Mater. Phys.* **1993**, *47*, 5485−5488.
(18) Goringe, C. M.; Bowler, D. R.; Hernandez, E. Tight-binding Modelling of Materials. *Rep. Prog. Phys.* **1997**, *60*, 1447−1512.
(19) von Neumann, J.; Wigner, E. P. Uber das Verhalten von Eigebwerten bei adiabatischen Prozessen. *Z.Physik* **1929**, *30*, 467−470.
(20) Landau, L. D.; Lifshitz, E. M. *Quantum Mechanics*; Pergamon: Oxford, U.K., 1981.
(21) Atkins, P.; de Paula, J. *Physical Chemistry for the Life Sciences*; Oxford University Press: Oxford, U.K., 2006.
(22) Zumdahl, S. S.; Zumdahl, S. A. *Chemistry*, 5th ed.; Houghton Miffin: Boston, 2000; p373.
(23) Rode, A. V.; Hyde, S.; Gamaly, E.; Elliman, R.; McKenzie, D.; Bulcock, S. Structural Analysis of a Carbon Foam Formed by High Pulse-rate Laser Ablation. *Appl. Phys. A: Mater. Sci. Process.* **1999**, *69*, S755−S758.
(24) Landau, L. D.; Lifshitz, E. M. *Statistical Physics Part I*; Pergamon: Oxford, U.K., 1980.
(25) Meyer, J. C.; Geim, A. K.; Katsnelson, M. I.; Novoselov, K. S.; Booth, T. J.; Roth, S. The Structure of Suspended Graphene Sheets. *Nature* **2007**, *446*, 60−63.
(26) Voevodin, V. V.; Zhumatiy, S. A.; Sobolev, S. I.; Antonov, A. S.; Bryzgalov, P. A.; Nikitenko, D. A.; Stefanov, K. S.; Voevodin, V. V. Practice of "Lomonosov" Supercomputer. *Open Systems J.* **2012**, *7*, 36−39 (In Russian).

DOI: 10.1021/acs.jpclett.5b02309
J. Phys. Chem. Lett. 2015, 6, 4525−4531